Wicking and Spreading of Water Droplets on Nanotubes

ARTICLE *in* LANGMUIR · FEBRUARY 2012

Impact Factor: 4.46 · DOI: 10.1021/la204073n · Source: PubMed

4 AUTHORS:

Ho Seon Ahn
Incheon National University
57 PUBLICATIONS **620** CITATIONS
SEE PROFILE

Gunyeop Park
Pohang University of Science and Technology
9 PUBLICATIONS **52** CITATIONS
SEE PROFILE

Joonwon Kim
Pohang University of Science and Technology
67 PUBLICATIONS **795** CITATIONS
SEE PROFILE

Moo Hwan Kim
Pohang University of Science and Technology
219 PUBLICATIONS **2,331** CITATIONS
SEE PROFILE

Langmuir

Article

pubs.acs.org/Langmuir

Wicking and Spreading of Water Droplets on Nanotubes

Ho Seon Ahn,[†] Gunyeop Park,[‡] Joonwon Kim,[‡] and Moo Hwan Kim*,[†]

[†]Division of Advanced Nuclear Engineering, POSTECH, Pohang, 790-784, Republic of Korea

[‡]Department of Mechanical Engineering, POSTECH, Pohang, 790-784, Republic of Korea

ABSTRACT: Recently, there has been intensive research on the use of nanotechnology to improve the wettability of solid surfaces. It is well-known that nanostructures can improve the wettability of a surface, and this is a very important safety consideration in regard to the occurrence of boiling crises during two-phase heat transfer, especially in the operation of nuclear power plant systems. Accordingly, there is considerable interest in wetting phenomena on nanostructures in the field of nuclear heat transfer. Much of the latest research on liquid absorption on a surface with nanostructures indicates that liquid spreading is generated by capillary wicking. However, there has been comparatively little research on how capillary forces affect liquid spreading on a surface with nanotubes. In this paper, we present a visualization of liquid spreading on a zircaloy surface with nanotubes, and establish a simple quantitative method for measuring the amount of water absorbed by the nanotubes. We successfully describe liquid spreading on a two-dimensional surface via one-dimensional analysis. As a result, we are able to postulate a relationship between liquid spreading and capillary wicking in the nanotubes.

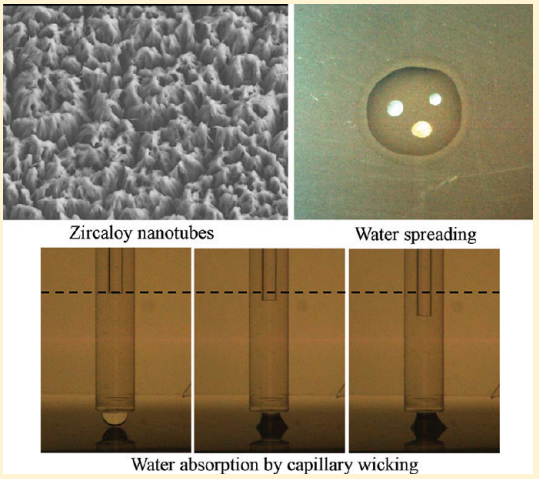

INTRODUCTION

Many applications involve the common fundamental process of liquid spreading on a solid surface. In these applications, the wetting behavior (wettability) varies according to the properties of the fluid and the solid surface, surface morphology, etc. The dominant governing factors in the wettability of a solid surface are surface energy and geometrical structures on the surface.[1−6] Intensive research has been devoted to the effect of nanostructures on the wettability of a surface.[7−11] Wetting phenomena of liquids on solid surfaces play an important role in the study of various applications, including heat pipes, self-cleaning glass, inkjet printing, and DNA chips.

In these days, new nanotechnologies applicable to the surface wettability have been introduced in a connection with the optimal surface for the nuclear fuel cladding.[12] The critical heat flux (CHF) or boiling crisis caused by heat transfer limitation and failure of heating material during the two-phase heat transfer is one of the most dangerous situations in a nuclear power plant. A number of studies have indicated that improved wettability of the heating surface strongly increases the CHF, and thereby enhances the operational safety of a nuclear power plant.[12−15] Therefore, there is much interest in understanding the wetting phenomenon on micro/nanoscale structures, which is directly related to CHF enhancement during boiling heat transfer, if the micro/nanoscale structures could be applied on the heating surface. However, existing studies of the effect of nanostructures on wetting have been mostly concerned with silicon substrates, rather than metal surfaces. Moreover, to increase the boiling heat transfer efficiency, there was an interesting study conducted using a multiwalled carbon nanotube array as a flat heater.[16] They postulated why the enhanced nucleate boiling heat transfer was the nanofin effect of the high thermal conductivity of carbon nanotubes.

According to our previous studies[12,13,15] about heat transfer application using nanofluids and micro/nanoscale structured heater surfaces, the capillary wicking with improved surface wettability strongly influences the CHF enhancement because the capillary wicking on the micro/nanoscaled structures played a role in replenishing the liquid on the dry-spot formation of the heater, finally delaying the CHF. The experimental results displayed well the CHF enhancement by the capillary pumping; however, its quantitative amount could not be estimated.

In the counterview of the heat transfer application, there have been few studies to understand the liquid spreading on the micro or nano scaled structures.[17,18] The water spreading on the micropillars could be characterized by the diameter of the wetted zone that surrounded the water droplet, which was also influenced by the diameter and the pitch of micropillars.[17] They[17,18] postulated that the movement of diameter of the wetted zone on the micropillars could be estimated by Washburn's law.[19] However, there was no description about the role of the water spreading by the capillary wicking between the micropillars.

In this study, a zircaloy surface (the material used in actual nuclear fuel cladding) was modified with arrays of nanotubes to improve its wettability. We observed dramatic changes in the surface structure. The wetting phenomena were influenced by the wicking of water in the arrays of nanotubes. Through a simple experiment, we were able to understand the phenomenon

Received: September 14, 2011
Revised: December 23, 2011
Published: January 6, 2012

   dx.doi.org/10.1021/la204073n | *Langmuir* 2012, 28, 2614−2619

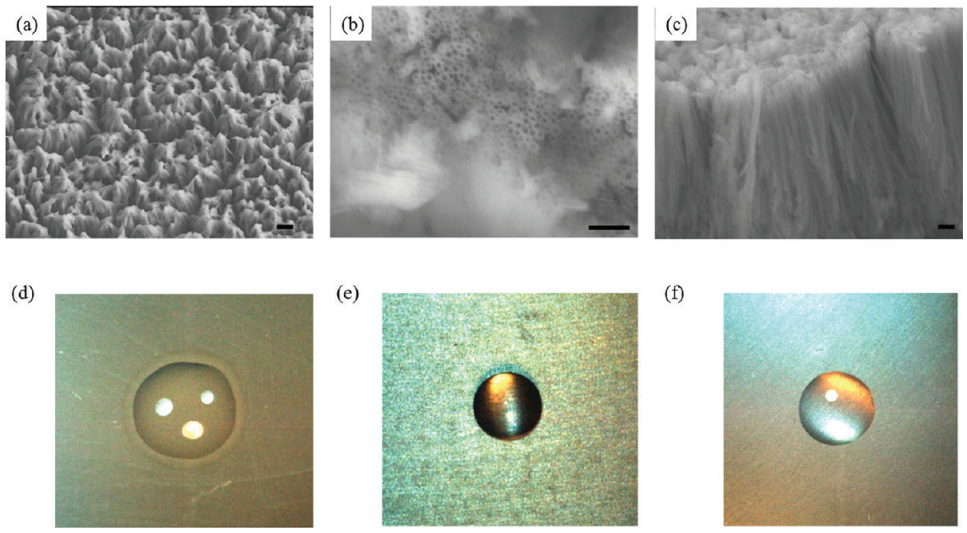

Figure 1. (a–c) SEM top view of the zircaloy surface with nanotubes. Arrays of the nanotubes. The scale bar is (a) 1 μm, (b) 100 nm, and (c) 100 nm, and panel c is the side view of the nanotubes in the vertical direction. (d) The precursor mark formed after droplet of 1.5 μL water was placed on the zircaloy surface with nanotubes. (e) The formation of a 1.5 μL water droplet on the bare zircaloy surface with a contact angle of 49°. (f) The formation of a 1.5 μL water droplet on the flat oxidized zircaloy surface with a contact angle of 16.2°.

of water spreading and quantitatively demonstrate improved wettability, water spreading, and capillary wicking on the nanotube arrays.

EXPERIMENTAL PREPARATION

The nanotubes were fabricated on the zircaloy surface (25 mm × 15 mm ×0.7 mm)[12] via the anodic oxidation technique. Prior to this, a polishing machine with #1000 silicon carbide abrasive paper was used to remove foreign substances from the surface. The remaining impurities were then removed in an ultrasonic bath, using a mixture of 50% acetone and 50% methanol for 1 h. The zircaloy surfaces were rinsed in deionized water and thoroughly blow-dried. A 0.5 wt % dilute HF solution was used as the electrolyte in the anodic oxidation process. A graphite plate was used as the counter-electrode for the anodic oxidation, and the electrodes were placed in parallel in the electrolyte with a spacing of 50 mm. A constant electric potential of 20 VDC was applied between the counter-electrode and the zircaloy surface. The temperature of the electrolyte was maintained at 10 °C throughout the reaction, using a circulating bath at constant temperature. The time required for anodic oxidation of the arrays of nanotubes was 6 min. According to our previous study,[12] the flat oxidized zircaloy surface was developed at the anodic oxidation from 40 s to 2 min. In this study, the contact angle of the flat oxidized zircaloy surface was 16.2° at the anodic oxidation time of 1 min. Following the anodic oxidation process, the zircaloy surfaces were rinsed with deionized water and thoroughly dried in a convection oven at 200 °C for 1 h, in order to remove the fluoride residue.

Scanning electron microscopy (SEM) images of the top view of the zircaloy nanotubes are shown in Figure 1. The nanotubes were aligned in the vertical direction (Figure 1a– c). The nanotubes had an average diameter of 20 ± 3 nm and an average height of 1.62 ± 0.21 μm throughout the top-view and tilt-view (45°) images shown in Figure 1b,c. The nanotube arrays exhibited superhydrophilic wetting (complete wetting), with a measured contact angle of 4.2 ± 2.3°. During the contact angle measurement, an interesting phenomenon was observed: once a water droplet touched the surface of the nanotubes, the precursor rim spread further than the contact line of the droplet, as shown in Figure 1d. As shown in Figure 1e,f, the water droplet formed without the precursor rim on the bare and flat oxidized zircaloy surfaces. This means that water droplets are quickly absorbed by nanotube arrays on a zircaloy surface. The layer of liquid spreading over the nanostructures is called the absorbed layer.[10,11] According to our previous study,[13] we have postulated that liquid spreading provides the active mode for liquid absorption by the nanostructures. However, we were unable to explain the mechanism of liquid suction in the nanostructures during spreading. Therefore, we designed a new and simple experimental method to estimate the amount of water in the absorbed layer. It is also known that liquid spreading on nanostructures is generated by capillary wicking between the liquid and the nanoscale morphology of the surface. What remains unclear is exactly how capillary wicking influences liquid spreading on the nanostructures of a two-dimensional surface. In this study, we explain the mechanism of liquid spreading due to capillary wicking, and estimate the amount of absorbed water in the nanotubes.

EXPERIMENTAL RESULTS AND DISCUSSION

We begin with a visualization of liquid spreading on the nanotubes. Figure 2 shows still images taken from a liquid spreading video with increasing time (sampling rate = 1000 frames/s). The figure also shows the three-phase contact line and precursor rim of the water droplet. At t = 0 ms, the water droplet was just above the surface. The droplet then contacted the surface, and was fully settled on the surface at t = 5 ms. The contact line of the droplet continued to spread, and at t = 100 ms, an additional rim (known as the precursor rim) appeared ahead of the apparent contact line. However, the precursor rim was initially so close to the contact line that it was difficult to distinguish between them. After further spreading of the droplet, at t = 200 ms, the precursor rim was advanced well ahead of the contact line. The diameters of both the contact line and the precursor rim increased with time until t = 1000 ms, when the contact line reached a maximum diameter. The precursor rim continued to expand, and reached a maximum at t = 3000 ms. Figure 2 indicates that both the contact line and the precursor rim were almost circular, which means that the zircaloy nanotubes were uniform, which was the primary assumption in this study. Empirical time correlations of the precursor rim diameter have been developed to interpret water spreading. On a flat surface, the radius $R(t)$ of the contact line obeys the dynamic scaling law $\pi R(t)^2 \sim t^n\Omega^p$, where t is time and Ω is the volume of the droplet.[20−22] Intermittently, the precursor rim was observed on the flat surface, which follow the diffusion law like $R_p \propto t^{1/2}$.[22] On a roughened surface, the wetted area (which is easily represented in terms of the radius) can be expressed

dx.doi.org/10.1021/la204073n | Langmuir 2012, 28, 2614–2619

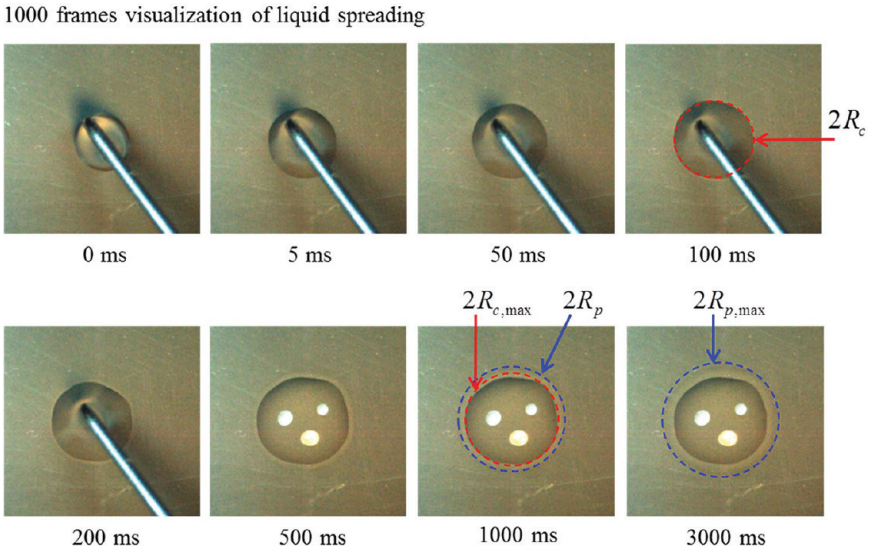

Figure 2. The snapshots of the spreading video at t = 0, 5, 50, 100, 200, 500, 1000, and 3000 ms. From the time of 100 ms during the water spreading, the contact line R_c and the precursor line R_p of the water droplet can be observed clearly. The contact line of the water droplet only appeared until t = 100 ms, and the precursor line appears soon. The contact line reaches the maximum at t = 1000 ms, but the precursor line continues expanding. The precursor line reaches the maximum at t = 3000 ms.

by $A/\Omega^{2/3} = k(t + \tau)^n$, where A is the wetted area, and k, τ, and n are empirical constants obtained from the best fit of experimental data.[23] Here, the precursor rim was also observed and followed the diffusion law $R_p \propto t^{1/2}$.[24] For a porous surface of the type considered in the present study, additional parameters such as pore size, pore density, and permeability are also important. Darcy's Law was used to develop the Washburn equation[19] $\delta = (R_e\gamma \cos\theta/2\mu)^{1/2}\sqrt{t}$, where δ is the stain penetration length corresponding to the radius, R_e is the effective radius of the capillary, and μ is the viscosity of the liquid.[25−28] The existing literature indicates that liquid spreading cannot be quantitatively expressed in terms of physical properties. However, the dynamics of the precursor rim could be represented by $R_p \propto t^{1/2}$.

To interpret the dynamics of the contact line and precursor rim during water spreading on the nanotubes, we used Washburn's Law ($L \sim C\sqrt{t}$)[19] to represent the dynamics of capillary wicking, where C is an empirical constant depending on the porosity, contact angle, surface tension, and geometrical curvature.[18] The diameters of the contact line ($D_c = 2R_c$) and precursor rim ($D_p = 2R_p$), averaged over the two perpendicular directions, were measured as functions of the spreading time, and are plotted in Figure 3. Both diameters appear to follow Washburn's Law reasonably well.[19] However, we divided the time domain into two stages. For t < 100 ms (short time), both D_c and D_p could be represented as monotonically increasing functions ($D \propto t$) with the same slope (Stage I in Figure 3, also referred to as the inertial regime by Quere[26]). For t > 100 ms, both D_c and D_p could be represented as increasing functions with square root proportionality ($D \propto t^{n/2}$) and different slopes, $n_c = 0.118 \pm 0.001$ and $n_p = 0.265 \pm 0.002$ (Stage II in Figure 3, which is in good agreement with previous results[11,19,21,22]). Stages I and II combined confirm the validity of Washburn's Law, since the root square function of time closely approximates the monotonic function in the very short time region (Stage I). In Stage I, the contact line and the precursor rim of the water droplet spread together. As previously mentioned, this is called the inertial regime,[26] and here the spreading of the water droplet was very rapid. In Stage II,

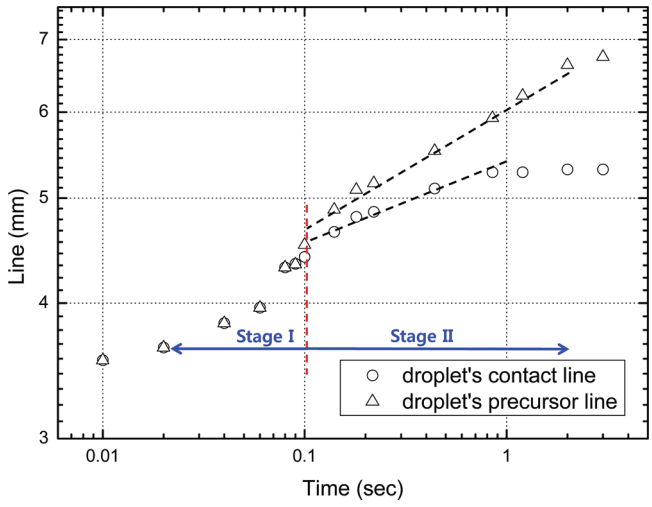

Figure 3. Variation of the contact line and precursor rim diameters with respect to time. In Stage I, both the contact line and precursor rim expand at the same velocity, $D \propto t$. However, in Stage II, the contact line stops expanding, and the precursor rim continues to expand at a lower velocity than Stage I, $D \propto t^{n/2}$.

the precursor rim advanced well ahead of the contact line, since the diameter of the precursor rim increased while the diameter of the contact line remained relatively static. A possible explanation for this is capillary wicking in the numerous nanochannels that formed between the nanotubes.[11] This is called the friction dominant regime.

The question remains as to exactly how capillary wicking affects the spreading of the precursor rim on the nanotubes of a zircaloy surface. Up to now, there has been no way to represent the capillary wicking on a (two-dimensional) plate with nanostructures. As noted above, $D \propto t$ in Stage I and $D \propto t^{n/2}$ in Stage II express the experimental relationship between the diameter of the precursor rim and time, as shown in Figure 3. The spreading of the water droplet could be governed by two forces: the capillary force on the zircaloy nanotube surfaces,

dx.doi.org/10.1021/la204073n | Langmuir 2012, 28, 2614−2619

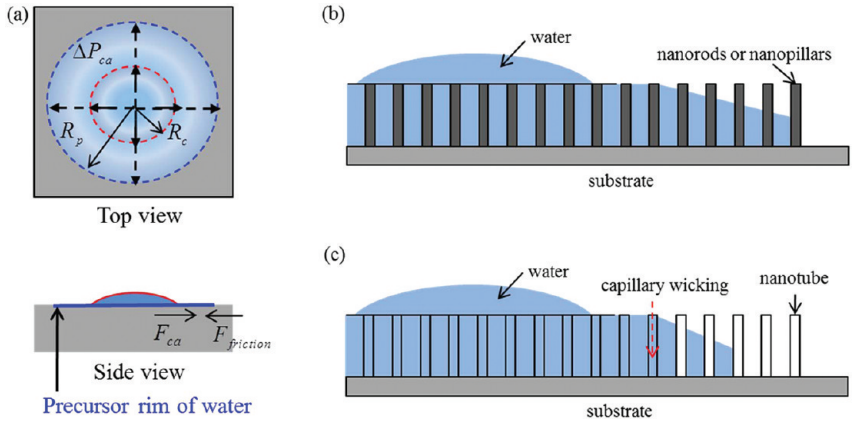

Figure 4. (a) Schematic diagram of water spreading under the relation between the capillary force and the friction force on the nanotubes. (b,c) Schematic diagram of the water spreading on the nanopillars and the nanotubes. Since the nanotube itself could absorb the water (according to the relation between the dispensed water amount and the precursor rim), the precursor rim (R_p) due to water spreading on the nanotubes would be weaker than nanopillars.

and the frictional force of the water flow. The capillary and frictional forces were expressed in the following simple form by Washburn:[19]

$$F_{ca} = C_1 R_{geometry} \sigma \cos\theta A_{area} = C_2 \Delta P_{ca} A_{area} \quad (1)$$

$$F_{friction} = B_1 \mu U R_p = B_1 \mu R_p \frac{dR_p}{dt} \quad (2)$$

where C_1, C_2, and B_1 are empirical constants, $R_{geometry}$ is the geometric curvature of the liquid, σ is the surface tension, θ is the contact angle, μ is the viscosity, U is the capillary velocity, A_{area} is the cross-sectional area, and R_p is the radius of the precursor rim during spreading. The schematic diagram to display eqs 1 and 2 is shown in the Figure 4a. The force balance on the plate can be applied to verify the effect of the capillary force on liquid spreading. The capillary force is determined by the constant capillary pressure (ΔP_{ca}) between nanotubes: $F_{ca} = \Delta P_{ca} \times A_{cross\_section}$ and $A_{cross\_section} = P\delta\varepsilon = 2\pi R_p \delta\varepsilon$, where $A_{cross\_section}$ is the cross-sectional area of the precursor rim, P is the perimeter of the precursor rim, δ is the thickness of nanotube array, and ε is the porosity of the zircaloy surface. The capillary pressure (ΔP_{ca}) is a constant value obtained from eq 1. In the very short time region ($t \sim 0$) of Stage I, there is an actual force due to the difference between the capillary and frictional forces ($F_{ca} > F_{friction}$), which generates the rapid spreading of the water droplet and concomitant significant increases in the diameters of both the contact line and the precursor rim. In the transitional region between Stage I and Stage II, the two forces are balanced ($F_{ca} = F_{friction}$). From eqs 1 and 2, the diameter of the precursor rim is given by a time expression of the form $R_p \sim B_2 t$, where B_2 is an empirical constant depending on the viscosity, the thickness of the microstructures, and the porosity. This expression, obtained from the visualization results, is in good agreement with the Stage I relationship $D \propto t$ mentioned above. In Stage II, there is an actual force due to the difference between the capillary and frictional forces ($F_{ca} < F_{friction}$), by which the precursor rim continues to spread gradually with decreased velocity. The above expression also is in good agreement with the relationship $D \propto t^{n/2}$ ($t > 100$ ms). Eventually, the liquid spreading ceases because of the limited volume of the dispensed water droplet. At this point, a new question arises: How does the nanotube array play a role in water spreading? Before further discussion, we re-examined the water spreading on the nanopillar and nanorod arrays. Figure 4b shows a schematic diagram of water spreading on the nanopillars. As determined in previous studies,[9−11,17] water can permeate into the spaces between the nanopillars in a process termed capillary invasion.[10] The precursor rim, which advances well ahead of the contact line, can be viewed as evidence that the water permeates the nanopillars in the other studies and the nanotubes in this study. If capillary wicking of water exists among nanotubes[29,30] (the oxidized zircaloy material is hydrophilic), water spreading on the nanopillars and nanotubes would be due to a different mechanism. As shown in Figure 4c, each nanotube plays a role as a water absorber. This means that water spreading on the nanotubes is weaker than on the nanopillars, because each nanotube can absorb a certain amount of water under the limited volume of the dispensed water droplet. Water absorption into the nanotubes and between the nanotubes in the array is also provided by capillary forces due to the water surface tension, the inner space of the nanotube, and the nanosized channels of the nanotube array. However, the direction would be perpendicular, and the vertical capillary force would play a role as the main triggering force for absorption at the initial (beginning) stage, when the water droplets first contact the nanotubes. The vertical capillary force into the nanotubes would absorb the water vertically, regardless of the horizontal water spreading caused by capillary forces between the nanotubes in the array. When the water spreading is complete, the spherical cap of the water droplet remains on the water film and plays a role in the water reservoir because of incomplete wetting (contact angle ~4.2°). As previously noted, the total volume of the dispensed water droplet is important in determining the ability of water spreading. For further research, we recommend a quantitative comparison of water spreading on the nanopillars and the nanotubes for a case in which the diameter, pitch, height, and material of pillars and tubes are the same.

We conducted a simple experiment in order to confirm the theoretical approach of the precursor rim during the water spreading and to estimate the amount of liquid absorbed by the nanotube surfaces. Figure 5 shows a schematic diagram of the experimental apparatus and a captured image of the initial state. A microtube (PFA) with an inner diameter of 500 μm was used for the capillary tube. A total of 1.5 ± 0.1 μL of deionized water was used, including the pensile droplet, as indicated in Figure 5. A micro support jack was used to elevate the test surface just

dx.doi.org/10.1021/la204073n | Langmuir 2012, 28, 2614−2619

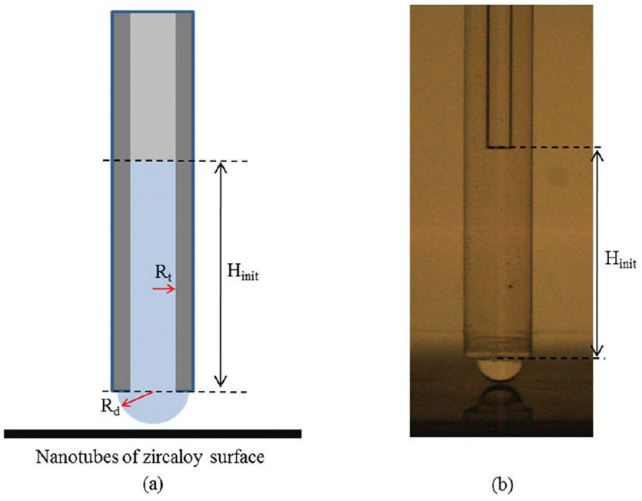

Figure 5. (a) Schematic diagram of the wicking measurement apparatus consisting of a capillary tube (the suggested value of the inner diameter was 500 μm, and the measured value was 492 μm) with a pensile water droplet. (b) Initial state of the capillary tube and pensile water droplet. Using image processing based on the reference image with the pensile water droplet, the total liquid volume was estimated at 1.42 μL, which is more accurate than the preinsertion of water with a microsyringe (1.5 μL).

enough to make contact with the pensile droplet suspended from the capillary tube. Water absorption by the nanotube surfaces was captured with a high-speed camera at 1000 frames per second. All images were processed to measure the height of the water in the capillary tube at every instant. Since the diameter of the capillary tube was known, this height was used to estimate the amount of absorbed water and its differential value over time. These estimates were also interpreted as representing the amount of water wicked in the nanotube arrays. Figure 5 shows still images of the liquid absorption with increasing time. From Figure 6a,b,c, the total water volume in the nanotube arrays was estimated at 1.5 μL. The height and volume of the water in the capillary tube in the initial state were H_{init} and $V_{init} = \pi R_t^2 H_{init}$, where R_t is the diameter of the capillary tube. More generally, the volume of water in the capillary tube at any time can be given by $V = \pi R_t^2 H$, where H is the height of the water in the capillary tube. Figure 7 shows the volume of water absorbed in the nanotubes of the zircaloy surface relative to time. The plot of the absorbed water as a function of time is very similar to the theoretical curve of Washburn's law. Actually, the volume of water in the capillary tube could represent the volume of water absorbed in the nanotubes of the zircaloy surface because of the continuity of the liquid column: $V_{absorbed} = V_{init} - V = V_{init} - \pi R_t^2 H$. The volume of absorbed water can also be divided into two stages over the total time range: Stage I ($V \propto t$ and $H \propto t$ for $t <$ 100 ms) and Stage II ($V \propto t^{n/2}$ and $H \propto t^{n/2}$ with $n = 0.279 \pm 0.027$ for $t >$ 100 ms). This indicates that two-dimensional liquid absorption in the nanotubes during water spreading can be estimated from one-dimensional liquid absorption using a capillary tube. Moreover, these results are in good agreement with the precursor rim observations during water spreading. In

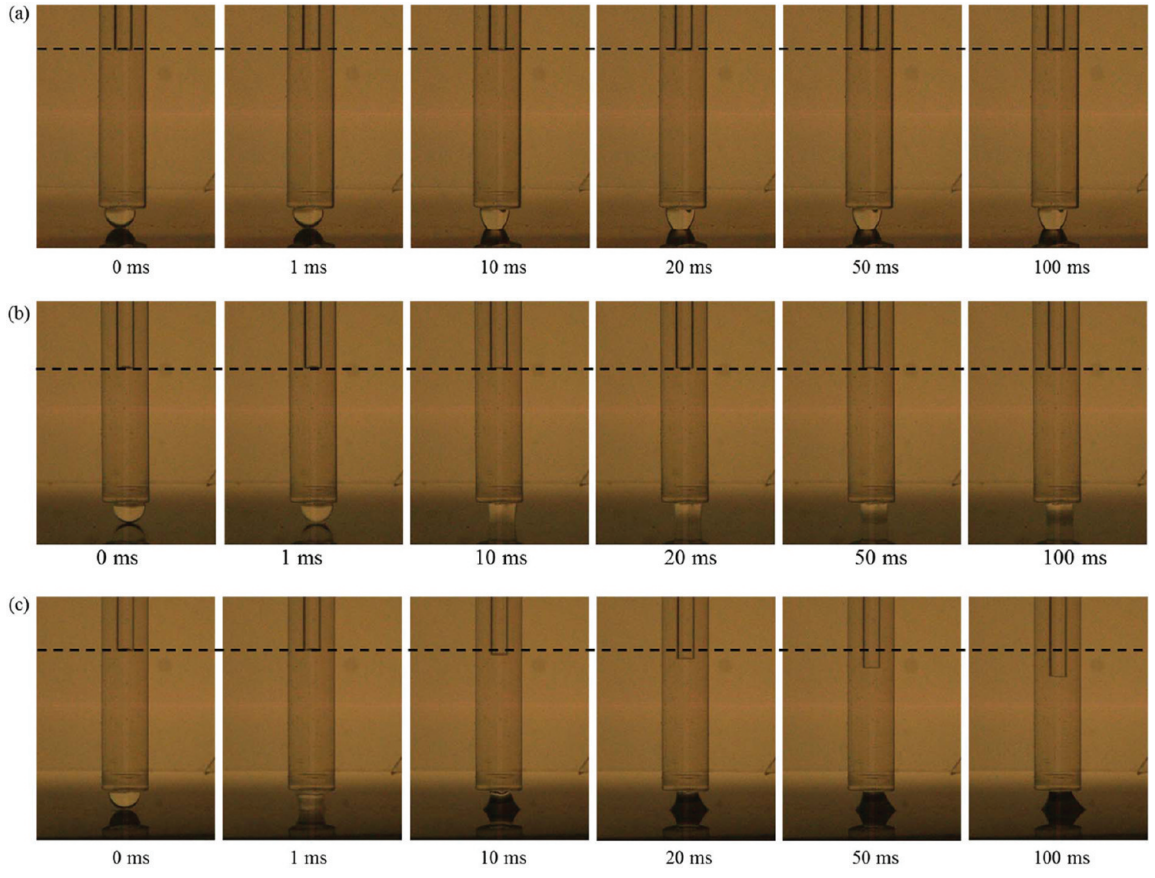

Figure 6. The liquid absorption on (a) a bare zircaloy surface, (b) the flat oxidized zircaloy, and (c) nanotubes of zircaloy surface as time increased. (a) and (b) show that the bare zircaloy surface has no liquid absorption. However, (c) shows the zircaloy with the zircaloy nanotubes absorb the liquid well, so that the height of the liquid inside of the micro tube is decreasing.

dx.doi.org/10.1021/la204073n | *Langmuir* 2012, 28, 2614–2619

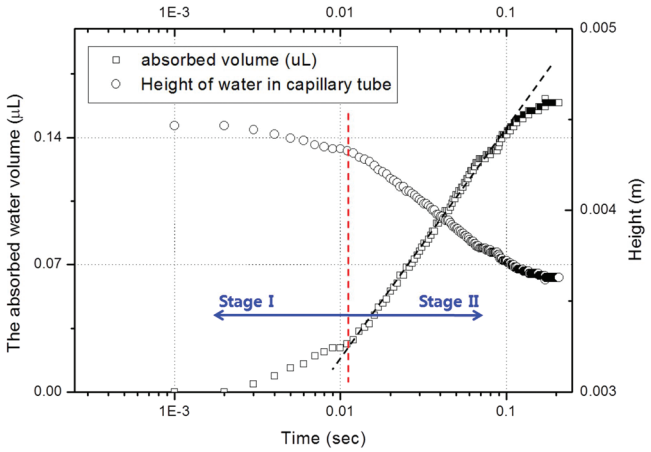

Figure 7. Volume of absorbed water in the nanotubes with respect to time. In Stage I, the amount of water absorbed increases according to the relationships $V \propto t$ and $H \propto t$. On the other hand, in Stage II, it increases gradually according to the relationships $V \propto t^{n/2}$ and $H \propto t^{n/2}$.

Stage I, the capillary force of the nanotubes is dominant, so that the water in the capillary tube is absorbed immediately at a constant absorption speed ($F_{ca} > F_{friction}$ and $F_{ca} = F_{friction}$), as with the diameter of the precursor rim during water spreading. In Stage II, the frictional force in the capillary tube and the nanotubes is dominant, so that the volume of absorbed water decreases gradually. The value of n is nearly the same as the value for the precursor rim during water spreading. This result indicates that one-dimensional analysis using a capillary tube is appropriate for representing water flow in the nanotubes during water spreading (which is equivalent to analyzing the precursor rim in terms of two-dimensional liquid absorption in the nanotubes, as noted above).

CONCLUSION

In this study, we successfully described capillary wicking and spreading of water on a nanotube surface, using a visualization of water droplet spreading and direct measurement of water absorption with a capillary tube. It was postulated that water spreading in the nanotubes (precursor rim) could be explained in terms of capillary wicking in the nanotubes. In addition, the volume of absorbed water in the nanotubes was estimated quantitatively, and it was also suggested that the volume of absorbed water could represent the amount of water in the precursor rim during water spreading.

AUTHOR INFORMATION

Corresponding Author

*Address: Division of Advanced Nuclear Engineering POSTECH Pohang, 790-784, South Korea. Tel: +82-54-279-2165. Fax: +82-54-279-3199. E-mail: mhkim@postech.ac.kr.

ACKNOWLEDGMENTS

This research was supported by the World-Class University (WCU) program through the National Research Foundation of Korea, funded by the Ministry of Education, Science, and Technology (R31-30005).

REFERENCES

(1) Young, T. *Philos. Trans. R. Soc.* **1985**, *95*, 65.
(2) Wenzel, R. N. *Ind. Eng. Chem.* **1936**, *28*, 988.
(3) Cassie, A. B.; Baxter, S. *Trans. Faraday Soc.* **1944**, *40*, 546.
(4) Johnson, R. E.; Dettre, R. H. *Adv. Chem.* **1963**, *43*, 112.
(5) Kim, D.; Kim., J.; Hwang, W. *Surf. Sci.* **2006**, *600*, 301.
(6) Marmur, A. *Langmuir* **2008**, *24*, 7573.
(7) Love, J. C.; Gates, B. D.; Wolfe, B. D.; Kateri, E. P.; Whitesides, G. M. *Nano Lett.* **2002**, *2*, 891.
(8) Lau, K. K. S.; Bico, J.; Teo, K. B. K.; Chhowalla, M.; Amaratunga, G.A. J.; Milne, W. I.; McKinley, G. H.; Gleason, K. K. *Nano Lett.* **2003**, *3*, 1701.
(9) Fan, J. G.; Tang, X.; Zhao, Y. P. *Nanotechnology* **2004**, *15*, 501.
(10) Fan, J. G.; Dyer, D.; Zhang, G.; Zhao, Y. P. *Nano Lett.* **2004**, *4*, 2133.
(11) Fan, J. G.; Zhao, Y. P. *Appl. Phys. Lett.* **2007**, *90*, 013102.
(12) Ahn, H. S.; Lee, C.; Kim, H.; Jo, H. J.; Kang, S. H.; Kim, J.; Shin, J.; Kim, M. H. *Nucl. Eng. Des.* **2010**, *240*, 3350.
(13) Ahn, H. S.; Jo, H. J.; Kang, S. H.; Kim, M. H. *Appl. Phys. Lett.* **2011**, *98*, 071908.
(14) Kim, S. J.; Bang, I. C.; Buongiorno, J.; Hu, L. W. *Appl. Phys. Lett.* **2006**, *89*, 153107.
(15) Kim, H. D.; Kim, M. H. *Appl. Phys. Lett.* **2007**, *91*, 014104.
(16) Ahn, H. S.; Sinha, N.; Zhang, M.; Banerjee, D.; Fang, S.; Baughman, R. H. *ASME Trans. J. Heat Transfer* **2006**, *128*, 1335.
(17) Ishino, C.; Reyssat, M.; Reyssat, E.; Okumura, K.; Quere, D. *Europhys. Lett.* **2007**, *79*, 56005.
(18) Chen, Y.; Melvin, L. S.; Rodriguez, S.; Weislogel, M. M. *Microelectron. Eng.* **2009**, *86*, 1317.
(19) Washburm, E. W. *Phys. Rev.* **1921**, *17*, 273.
(20) Tanner, L. H. *J. Phys. D* **1979**, *12*, 1473.
(21) de Gennes, P. G. *Rev. Mod. Phys.* **1985**, *57*, 827.
(22) Lopez, J.; Miller, C. A.; Ruckenstein, E. J. *Colloid Interface Sci.* **1976**, *56*, 460.
(23) Apel-Paz, M.; Marmur., A. *Colloids Surf., A* **1999**, *146*, 273.
(24) Cazabat, A. M.; Stuart, M. A. C. *Prog. Colloid Polym. Sci.* **1987**, *74*, 69.
(25) Kissa, E. J. *Colloid Interface Sci.* **1981**, *83*, 265.
(26) Starov, V. M.; Kosvintsev, S. R.; Sobolev, V. D.; Velarde, M. G.; Zhdanov, S. A. J. *Colloid Interface Sci.* **2002**, *246*, 372.
(27) Starov, V. M.; Kosvintsev, S. R.; Sobolev, V. D.; Velarde, M. G.; Zhdanov, S. A. J. *Colloid Interface Sci.* **2002**, *252*, 397.
(28) Quere, D. *Europhys. Lett.* **1997**, *39*, 533.
(29) Whitby, M; Quirke, N. *Nat. Nanotechnol.* **2007**, *2*, 87.
(30) Dimitov, D. I.; Milchev, A.; Binder, K. *Phys. Rev. Lett.* **2007**, *99*, 054051.